Developmental Cell
Article

Kinocilia Mediate Mechanosensitivity in Developing Zebrafish Hair Cells

Katie S. Kindt,[1] Gabriel Finch,[1] and Teresa Nicolson[1,*]
[1]Howard Hughes Medical Institute, Oregon Hearing Research Center, 3181 SW Sam Jackson Park Road, Oregon Health and Science University, Portland, OR 97239, USA
*Correspondence: nicolson@ohsu.edu
http://dx.doi.org/10.1016/j.devcel.2012.05.022

SUMMARY

Mechanosensitive cilia are vital to signaling and development across many species. In sensory hair cells, sound and movement are transduced by apical hair bundles. Each bundle is comprised of a single primary cilium (kinocilium) flanked by multiple rows of actin-filled projections (stereocilia). Extracellular tip links that interconnect stereocilia are thought to gate mechanosensitive channels. In contrast to stereocilia, kinocilia are not critical for hair-cell mechanotransduction. However, by sequentially imaging the structure of hair bundles and mechanosensitivity of individual lateral-line hair cells in vivo, we uncovered a central role for kinocilia in mechanosensation during development. Our data demonstrate that nascent hair cells require kinocilia and kinocilial links for mechanosensitivity. Although nascent hair bundles have correct planar polarity, the polarity of their responses to mechanical stimuli is initially reversed. Later in development, a switch to correctly polarized mechanosensitivity coincides with the formation of tip links and the onset of tip-link-dependent mechanotransduction.

INTRODUCTION

Hair cells are the specialized mechanosensory receptors of the auditory and vestibular systems that convert head movements and sound waves into electrical signals (reviewed in Schwander et al., 2010). Projecting from the apical surface of each hair cell is a stiff hair bundle, consisting of rows of interconnected stereocilia tethered to a single kinocilium. Stereocilia are densely packed with actin filaments and form parallel rows that increase progressively in height, creating a staircase-like structure; adjacent to the tallest row of stereocilia is the kinocilium, a true cilium with a 9 + 2 arrangement of microtubules. Cadherin 23 (Cdh23) and Protocadherin 15 (Pcdh15) form extracellular tip links that connect adjacent rows of stereocilia, as well as kinocilial links that tether the tallest row of stereocilia to the kinocilium (Ahmed et al., 2006; Goodyear and Richardson, 2003; Siemens et al., 2004; Söllner et al., 2004). This morphological polarity, a stereocilia-based staircase leading to the kinocilium, is believed to restrict functional polarity, or hair-cell mechanosensitivity, to a single direction of bundle deflection (Shotwell et al., 1981). Deflection of the hair bundle toward the kinocilium is thought to tension tip links and open mechanosensitive channels, depolarizing the hair cell (Pickles et al., 1984). Conversely, deflection away from the kinocilium is thought to relieve tip-link tension and close mechanosensitive channels.

During hair-cell development, the kinocilium is the first structure to appear on the apical cell surface (Denman-Johnson and Forge, 1999; Tilney et al., 1992). Subsequently, rows of stereocilia emerge progressively and elongate adjacent to the kinocilium. Stereocilial elongation is accompanied by the addition of mechanotransduction components, including tip links. Hair bundles at this stage—comprising a full complement of stereocilia correctly polarized in a staircase formation, with detectable tip links—mark the onset of functionally polarized mechanotransduction currents (Géléoc and Holt, 2003; Lelli et al., 2009; Si et al., 2003). In auditory hair cells of mammals and birds, kinocilia regress soon after the onset of mechanotransduction, whereas vestibular hair cells maintain kinocilia throughout maturity (Denman-Johnson and Forge, 1999; Kikuchi and Hilding, 1966; Tanaka and Smith, 1978).

Although kinocilia are retained in mature vestibular hair cells, their exact role remains unclear. Previously, it had been hypothesized that the kinocilium may have a mechanosensitive function, but currently, there is no evidence to support this idea (Engström et al., 1962; Hillman, 1969; Shin et al., 2005). Rather, removal of the kinocilium from mature bullfrog vestibular hair cells does not affect mechanotransduction currents, suggesting that the kinocilium plays no role in mechanosensation (Hudspeth and Jacobs, 1979). This lack of function is in contrast to mammalian ciliated mechanosensory cells, and to invertebrate and flagellate mechanoreceptors, where cilia act as direct sensors of extracellular mechanical signals (Fujiu et al., 2011; Kahn-Kirby and Bargmann, 2006; McGrath et al., 2003; Nauli et al., 2003; Walker et al., 2000).

Because all hair cells initially have kinocilia, we hypothesized that kinocilia may have a mechanosensitive function during development. To study kinocilial function during development, we applied in vivo imaging of hair-cell activity and structure in conjunction with scanning electron microscopy (SEM). Surprisingly, we find that hair cells are mechanosensitive much earlier than previously reported—before FM 1-43 label and tip links are detectable. In these nascent hair cells, however, functional polarity is reversed relative to hair-bundle morphological polarity. Furthermore, we show that hair cells require a kinocilium and kinocilial links for these nascent responses, providing

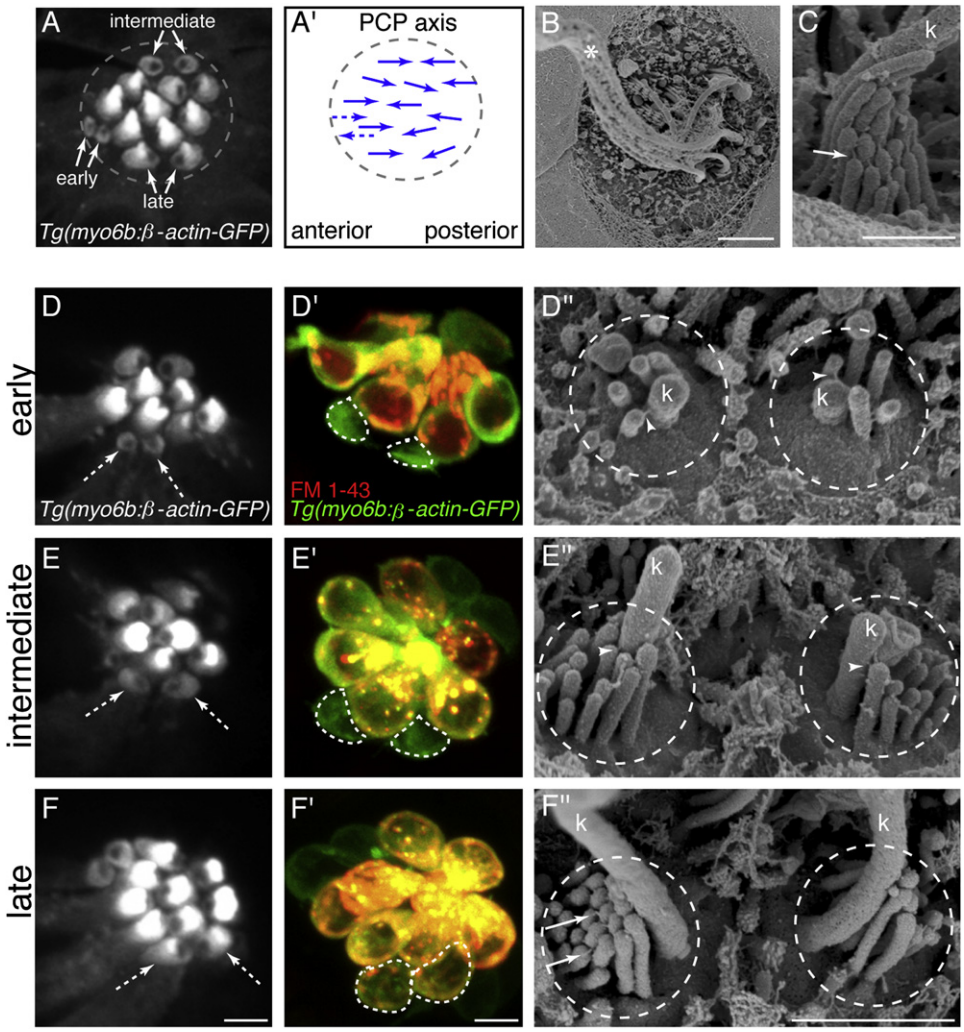

Figure 1. Direct Comparison of Hair-Bundle Development Using Transgenic *β-actin-GFP*, FM 1-43, and SEM

(A) Top-down view of neuromast hair bundles labeled with *Tg(myo6b:β-actin-GFP)*. Three stages of immature hair-bundle development can be observed: early, intermediate, and late. The unlabeled region on either the caudal or rostral side of each bundle is the insertion point of the kinocilium.

(A′) Arrows indicate planar polarity and functional polarity of hair bundles in (A). Dashed arrows indicate predicted planar polarity. PCP, planar cell polarity.

(B) SEM image of a neuromast at 3 dpf; asterisk denotes the many tall kinocilia (k).

(C) SEM image of a mature hair bundle.

(D, E, and F) Confocal images of hair bundles expressing *β-actin-GFP*. White dashed arrows indicate hair bundles of respective stage examined.

(D′, E′, and F′) White dashed lines outline cell bodies after FM 1-43 label of hair bundle examined in (D), (E), and (F).

(D″, E″, and F″) SEM images of hair bundles in (D), (E), and (F).

All images were taken at 3 dpf. White arrowheads denote kinocilial links; solid white arrows denote tip links. Anterior is left; dorsal is up. Scale bars, 2.5 μm (A, B, D, E and F), 500 nm (C), 5 μm (D′, E′, and F′), and 1 μm (D″, E″, and F″). See also Figure S1.

substantial evidence that kinocilia have mechanosensitive function in hair cells.

RESULTS

Direct Comparison of Hair-Bundle Development and Function by Confocal and Electron Microscopy

To examine the function of kinocilia during development, we utilized the zebrafish posterior lateral-line organ, which is an auxiliary sensory organ present in fish and amphibians, specialized for local water flow detection. The lateral line consists of superficial clusters of hair cells called neuromasts, arranged along the length of the animal (Figures 1A, 1B, 3A, and 3D). Hair cells of the lateral-line organ are born in pairs, and sister hair cells adopt opposing polarities along the anterior-posterior (A-P) axis of the fish (López-Schier et al., 2004; Seiler et al., 2005) (Figure 1A). The morphological and planar polarity of a given hair bundle is determined by the asymmetric localization of the actin-rich stereocilia relative to the kinocilium (Figures 1A and 1A′; see Figures S1A and S1A′ available online).

For our study, we first developed a basic framework for characterizing the various stages of development in terms of

Table 1. Quantification of the Morphological and Functional Development of Zebrafish Hair Cells

	Early		Intermediate		Late		Mature	
Hair-Bundle Morphological Development								
Kinocilium height (μm)	0.33 ± 0.03		1.07 ± 0.09		5.20 ± 0.54		14.42 ± 0.50	
Bundle height (μm)	0.26 ± 0.01		0.49 ± 0.04		0.77 ± 0.04		1.42 ± 0.06	
Rows of stereocilia	1.6 ± 0.1		3.0 ± 0.1		3.6 ± 0.1		4.4 ± 0.1	
Number of hair cells	25		25		25		25	
Polarized Responses in Developing Hair Cells								
Genotype	WT	*ift88*	WT	*ift88*	WT	*ift88*	WT	*ift88*
Negative	74%	6%	27%	6%	–	–	–	–
Bidirectional	–	–	24%	–	49%	–	4%	–
Positive	11%	–	29%	11%	46%	27%	94%	71%
No response	15%	94%	20%	83%	5%	73%	2%	29%
Number of FM 1-43-labeled hair cells	0	0	28[a]	2[b]	39	15	51	21
Number of hair cells	47	18	51	18	39	15	51	21

±, SEM; –, no observed response.
[a]Eleven bidirectional, 13 positive, 4 no response.
[b]Two positive.

morphology and function. To accomplish this in vivo, we generated transgenic fish expressing *β-actin-GFP* under control of a hair-cell-specific *myo6b* promoter and used confocal microscopy to image actin-GFP in hair bundles (Figures 1A–1F). These animals were then assessed for mechanosensitivity with FM 1-43, a vital dye that labels hair cells with functional mechanotransduction channels (Gale et al., 2001) (Figures 1D′–1F′). Finally, ultrastructural features of the same hair bundles were examined using SEM (Figures 1D″–1F″).

The results of in vivo imaging followed sequentially by SEM revealed multiple stages of hair-bundle development within each neuromast. We therefore categorized stages of hair-bundle development. Hair bundles were defined as mature or immature, and immature hair bundles were further subclassified as early, intermediate, or late (Figures 1A and 1D–1F″). Actin localization showed that early hair bundles had a thin and uniform circumferential actin ring at the hair-cell surface. High-resolution SEM analysis revealed that these early bundles had one or two rows of stereocilia at a height roughly equal to the kinocilium (Figures 1D and 1D″; Table 1). Interestingly, early sister hair cells had correct planar polarity relative to each other and to the A-P axis of the fish (Figures 1D″ and S1C). Any minor misalignments in early bundle were comparable to those observed in mature bundles (Figure S1C). At the intermediate stage, actin localization reflected an established morphological polarity, and SEM showed that on average, three rows of stereocilia were present. In these intermediate bundles, the height of stereocilia was double that of early bundles, and the kinocilium was twice the height of the tallest stereocilia (Figures 1E and 1E″; Table 1). Late-stage hair bundles showed a further increase in height, had three to four rows of stereocilia, and a kinocilium that was at least five times the height of the tallest stereocilia (Figures 1F and 1F″; Table 1). Only late-stage hair bundles consistently labeled with FM 1-43 and had detectable tip links in SEM images (Figures 1F′ and 1F″). This is in agreement with previous studies correlating FM 1-43 label with the presence of tip links and the onset of mechanosensitivity in mouse and chick hair cells (Géléoc and Holt, 2003; Si et al., 2003). Finally, mature hair bundles had between four and five rows of stereocilia, a bundle height of approximately 1.5 μm, and a kinocilial height of 14 μm (Figure 1C; Table 1). This coordinated approach provided a fundamental reference for the development of hair-bundle morphology and the onset of mechanosensitive function that we applied to subsequent analyses.

Loss of Kinocilia Does Not Disrupt Hair-Bundle Development

Upon establishing methods to track and categorize the stages of hair-bundle development, we then examined the role of kinocilia in the onset of mechanosensitivity. For this analysis, we characterized *ovl/ift88* mutants that lack normal kinocilia (Tsujikawa and Malicki, 2004). Using SEM and immunohistochemistry, we confirmed that in *ift88*^{tz288b} mutants kinocilia were severely stunted (mature kinocilia length: 14.42 μm in wild-type, n = 25; 0.29 μm in *ift88*^{tz288b}, n = 11; Figures 2A–2D). We occasionally observed slightly elongated (>5 μm) kinocilia in younger larvae (2 days postfertilization [dpf]), but never kinocilia that were mature in length (data not shown). This is consistent with previous reports using a maternal zygotic *ift88* mutant that suggest in younger larvae there is residual *ift88* maternal RNA in *ift88*^{tz288b} mutants (Huang and Schier, 2009). Importantly, SEM images of *ift88*^{tz288b} hair bundles showed that whereas kinocilia were severely stunted in both immature and mature hair bundles, hair-bundle development was not affected (Figures 2A and 2B). In contrast to a study of auditory hair cells in mice, loss of Ift88 and kinocilia did not result in hair-bundle planar polarity defects (Figures 2C and 2D) (Jones et al., 2008). Normal planar polarity indicates that either the kinocilium is not required to establish the coordinated organization of zebrafish hair bundles or that in *ift88*^{tz288b} hair bundles, although severely stunted, kinocilia are still able to fulfill this role.

In addition to unaltered hair-bundle development, we observed that at 2 dpf, a stage when each neuromast contains

hair cells at multiple developmental stages—early, intermediate, late, and mature—*ift88*^{tz288b} mutant neuromasts had a similar number of hair cells compared to wild-type neuromasts (Figure 2E). Furthermore, we found that in *ift88*^{tz288b} mutant hair cells, FM 1-43 label progressed on a similar scale in developing hair cells as in wild-type larvae (Figures 2F and 2G), suggesting that a functional, developmental comparison was valid.

The Onset of Mechanosensitivity Precedes FM 1-43 Label and Requires Kinocilia

Normal labeling of mutant hair cells with FM 1-43 suggested that mechanotransduction was unaffected in *ift88*^{tz288b} larvae. In many species, labeling with FM 1-43 is an accepted method to assess hair-cell activity; however, using a second method for assessing physiological responses in parallel is more comprehensive. Previous studies of hair-cell mechanosensitivity in zebrafish have relied on measurements of extracellular microphonic potentials (Tanimoto et al., 2011; Trapani and Nicolson, 2011). Such recordings represent the sum response of all hair cells in a sensory patch. Because each neuromast contains hair cells at different stages (Figure 1), microphonic potentials are not suitable for determining the onset of mechanotransduction. We therefore developed a method to measure hair-cell activity at the resolution of single cells. For these experiments we generated transgenic fish expressing cameleon D3cpv (Palmer et al., 2006), a genetically encoded FRET (fluorescence resonance energy transfer)-based calcium indicator, in hair cells (Figures 3A and 3D).

Using intact transgenic larvae expressing cameleon, we first characterized the responses of wild-type hair cells to confirm that FM 1-43 labeling correlated with mechanosensitivity. For this analysis, we examined neuromasts at 5 and 2 dpf to compare populations of mature and immature hair cells, respectively (Figures 3A–3F). When stimulated along the A-P axis using a fluid jet, hair cells displayed robust mechanically evoked calcium responses. Subsequently, when we labeled cells with FM 1-43, we confirmed that the majority of cells at 5 and 2 dpf that labeled with FM 1-43 were mechanosensitive, as defined by a rise in intracellular calcium levels (5 dpf: 94%, n = 128 cells; 2 dpf: 84%, n = 44 cells).

When we extended our analysis to the immature, FM 1-43-unlabeled cells at 2 dpf, we made a striking observation. In contrast to previous studies, we reproducibly detected mechanosensitive calcium responses in cells that did not label with FM 1-43 (Figures 3D–3F, cell 1; Figure 3G: 67%, n = 39 cells). It should be noted that the responses of FM 1-43-unlabeled cells were significantly smaller than responses of FM 1-43-labeled cells (Figure 3G). Although smaller, mechanosensitive responses in FM 1-43-unlabeled cells were reliably detected over a wide range of fluid jet pressures, using numerous stimulus paradigms and also using a piezo-driven glass fiber to deflect hair bundles (Figures S2E, S2H, and S2I). Previous studies have shown that hair cells with incompletely assembled, improperly tensioned, or closed channels could be labeled by deflecting hair bundles in the presence of FM 1-43 (Lelli et al., 2009). However, we found that neither application of additional FM 1-43 nor sustained deflection in the presence of FM 1-43 could label immature FM 1-43-unlabeled cells that were mechanosensitive (Figures S4A–S4A‴ and S4B–S4B‴). These observations suggest that

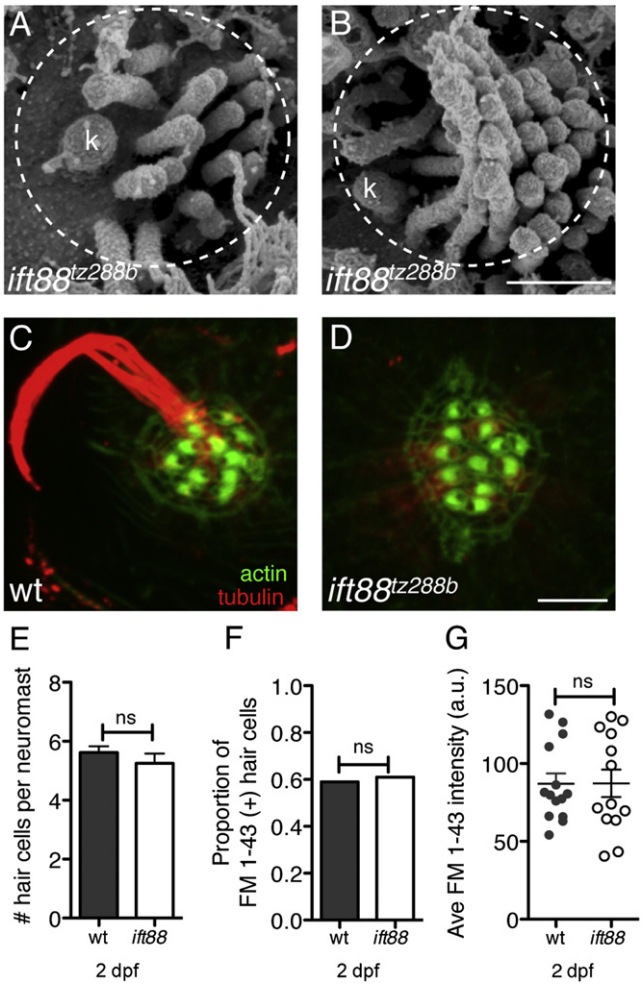

Figure 2. *ovl/ift88* Mutant Hair Cells Lack Kinocilia yet Develop Normally

(A and B) SEM image of an *ift88*^{tz288b} immature (A) and mature (B) hair bundle.

(C and D) Tubulin and actin stain of bundles at 5 dpf in wild-type (WT) (C) and *ift88*^{tz288b} (D).

(E) The average number of hair cells per neuromast at 2 dpf in wild-type and *ift88*^{tz288b} neuromasts (n > 13 neuromasts). ns, not significant.

(F) Proportion of FM 1-43-labeled hair cells in *ift88*^{tz288b} and wild-type neuromasts at 2 dpf (n > 13 neuromasts).

(G) The average FM 1-43 intensity per neuromast at 2 dpf (n > 13 neuromasts). a.u., arbitrary units.

An unpaired Student's t test was used to compare number of hair cells per neuromast in (E) and (G). A chi-square Fisher's exact test was used to compare proportion of FM 1-43-labeled hair cells in (F). Scale bars, 500 nm (A and B) and 5 μm (C and D). Error bars are SEM.

despite their lack of FM 1-43 label, immature responses are robust, and immature cells possess functional mechanosensitive channels.

Because the kinocilium is the first apical structure to appear in developing hair cells, one obvious question is whether the kinocilium is required for mechanosensitive responses in immature cells that do not label with FM 1-43. When we examined mechanically evoked calcium responses in *ift88*^{tz288b} mutants using our transgenic line expressing cameleon, we found that

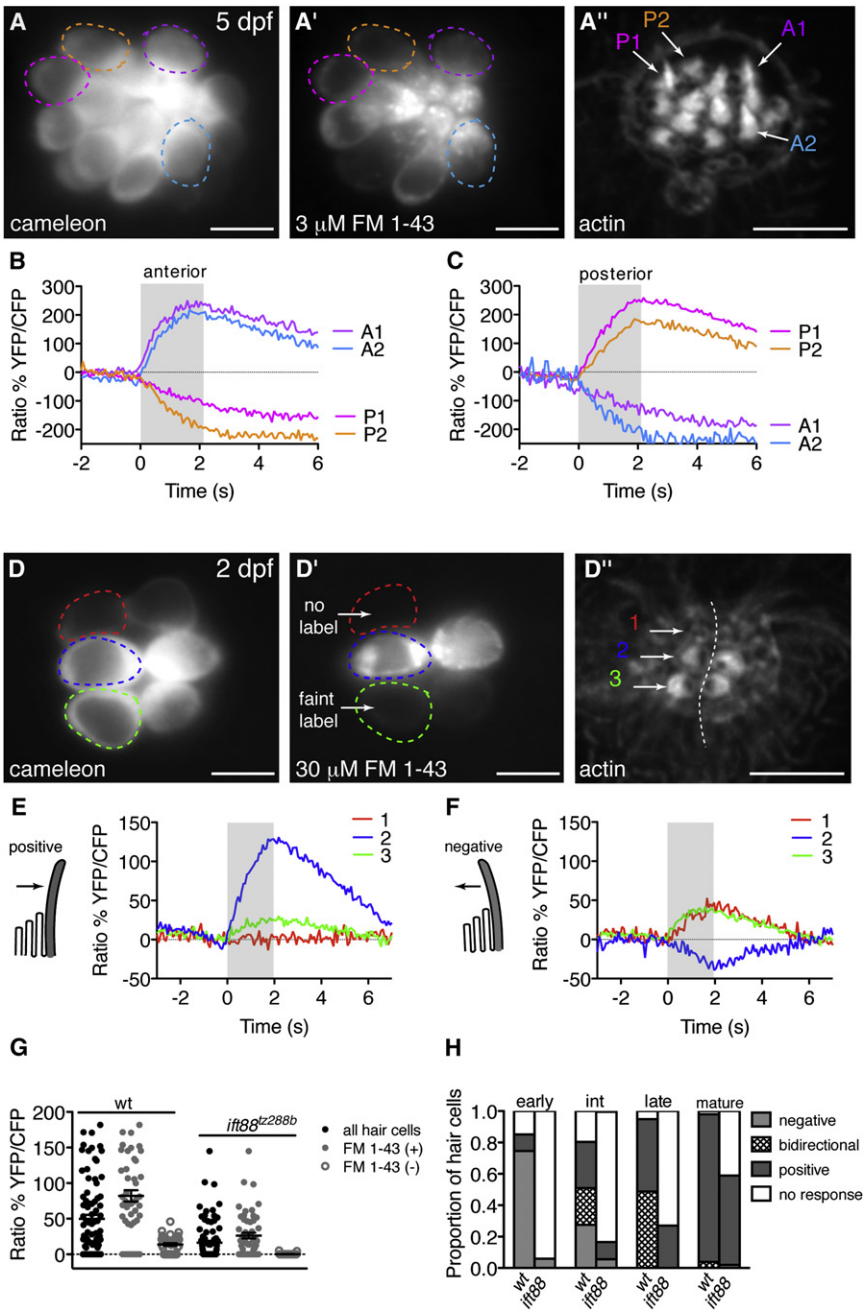

Figure 3. Functional Polarity of Mature and Immature Zebrafish Hair Cells

(A) A 5 dpf neuromast expressing cameleon. Circles represent cells analyzed and are color coded and correspond to data in (A′)–(C).

(A′ and A″) FM 1-43 and phalloidin stain of the neuromast in (A). Two anterior-polarized hair bundles (A1 and A2) and two posterior-polarized hair bundles (P1 and P2) are indicated.

(B and C) Response of four individual hair cells highlighted in (A) to the same anterior (B) and posterior (C) stimulus.

(D–D″) Same layout as (A)–(A″) except analysis is at 2 dpf. Hair cell stages are as follows: cell 1, early; cell 2, mature; cell 3, intermediate. (D) A neuromast expressing cameleon. (D′) FM 1-43 strongly labeled a pair of mature cells (cell 2 and sister), faintly labeled a pair of intermediate cells (cell 3 and sister), and yet did not label a pair of early hair cells (cell 1 and sister). (D″) Phalloidin label of the neuromast in (D)–(D′).

(E and F) Mechanically evoked calcium responses corresponding to cells 1–3. Negative and positive deflections are indicated with schematics. Kinocilium is denoted as the tall, gray structure. Cell 1 responded to only negative deflections. Cell 2 responded to positive deflections. Cell 3 responded to both negative and positive deflections.

(G) Hair-cell responses (black circles) from wild-type (n = 13 neuromasts) and *ift88*^{tz288b} (n = 21 neuromasts) at 2 dpf. These same data were broken down into FM 1-43-labeled hair cells (gray circles) and FM 1-43-unlabeled hair cells (open gray circles).

(H) Proportion of negative, bidirectional, and positive responses at 2 dpf (n = 188 wild-type and 72 *ift88*^{tz288b} cells).

Errors bars are SEM. Scale bars, 5 μm. For stimulus controls, see also Figure S2.

Morphological Polarity Does Not Accurately Predict Functional Polarity in Immature Hair Cells

To parse out the exact role of the kinocilia in the acquisition of mechanosensitivity, we characterized developing hair-cell responses in more detail. At 2 dpf, hair cells are positioned in a highly stereotyped fashion within each neuromast, along a line perpendicular to the axis of mechanosensitivity (Figure 3D″). Sister cells are paired across this line and are fated to have opposing polarities (Figure 3D″) (López-Schier et al., 2004). In this arrangement, when mature, all cells initially present on the left side of the neuromast will respond to posterior stimuli, and those on the right side will respond to anterior stimuli.

In line with this polarized arrangement, in mature cells at 2 dpf, deflection in the positive direction (toward the kinocilium) was accompanied by a rise in intracellular calcium levels (Figure 3E, cell 2), whereas deflection in the negative direction (away from the kinocilium) resulted in a decrease in intracellular calcium (Figure 3F, cell 2). When stained with phalloidin, the observed similar to wild-type cells, in *ift88*^{tz288b} mutants the majority of FM 1-43-labeled cells were mechanosensitive (Figure 3G: 71%, n = 55 cells). Of the *ift88*^{tz288b} cells that labeled with FM 1-43, the magnitude of the responses was significantly reduced (Figure 3G). However, in contrast to wild-type larvae, we observed that *ift88*^{tz288b} cells without FM 1-43 label were rarely mechanosensitive (Figure 3G: 6%, n = 35 cells). Relative to wild-type, the reduction in response size and loss of a subset of immature responses suggest that either full-length kinocilia are required for transmitting the forces of mechanical stimuli to the bundle or that kinocilia are intrinsically involved in mechanosensitivity during development.

functional polarity of each mature cell at 2 dpf correlated with the morphological planar polarity of its hair bundle (Figures 3D–3F, cell 2). Similar results were obtained at 5 dpf when the majority of neuromast hair cells are mature (Figures 3A–3C).

In contrast to mature cells, we observed that the functional polarity of FM 1-43-unlabeled cells was often completely reversed—FM 1-43-unlabeled, immature cells frequently showed an increase in intracellular calcium when stimulated in the negative direction (70% derived from Table 1 early and intermediate FM 1-43-unlabeled cells; Figure 3F, cell 1). Furthermore, in FM 1-43-labeled cells that were still immature, we observed a large subset that responded bidirectionally (increase in intracellular calcium to both negative and positive deflections) (45% derived from Table 1 intermediate and late FM 1-43-labeled cells; Figures 3B and 3C, cell 3). Inappropriate functional polarity was surprising because our SEM analysis of hair-bundle ultrastructure revealed that developing bundles had correct planar polarity, which is thought to be predictive of correct functional polarity (Figures 1 and S1C).

Because correct hair-bundle polarity did not correlate with functional polarity in developing cells, it was unclear whether functional polarity was restricted to the A-P axis as in mature cells. To test A-P axis restriction, we examined responses to stimuli oriented at 45° or 90° relative to the A-P axis (Figures S1D–S1G). We observed that in all cells, off-axis responses were substantially reduced (Figure S1D). Residual off-axis responses are likely due to the fact that many hair bundles, even mature ones, are not perfectly aligned along the A-P axis (Figures S1A–S1C). Importantly, the reduction in off-axis response was independent of developmental stage and FM 1-43 label, indicating that even the youngest developing hair cells are directionally restricted along the A-P axis (Figures S1D–S1G).

We also performed several controls to determine if the atypical functional polarity in immature hair cells was robust and reproducible. We found that similar results were observed for a range of fluid jet intensities and using a piezo-driven glass fiber to deflect hair bundles (Figures S2F and S2G). These results indicate that immature functional polarity is robust in response to stimulation with either glass fiber or fluid jet, and the signal generated correlates with the strength of the stimulus.

Functional Polarity Reverses during Hair-Bundle Development; Reversed Responses Require Kinocilia

After confirming the reproducibility of immature hair-cell responses, we next examined whether (1) the patterns of immature functional polarity we observed in wild-type larvae correlated with specific stages of hair-bundle development and (2) if kinocilia were required for atypical functional polarity at specific stages of development.

To test for a correlation between developmental stage and type of response, we first analyzed the functional polarity of individual developing hair cells at 2 dpf and then determined the developmental stage of each cell based on kinocilial length, FM 1-43 label, and localization of actin-rich bundles (Figures 3D–3D″). Using this approach, we identified a complete reversal of functional polarity during hair-bundle development (Figure 3H; Table 1). Immature early cells predominantly responded to negative deflections and did not label with FM 1-43 (Figure 3H; Table 1: 75% negative, 11% positive, 15% no response, n = 47). The functional polarity of intermediate cells was more heterogeneous (Figure 3H; Table 1: 27% negative, 24% bidirectional, 29% positive, 20% no response, n = 51), and nearly half of the cells labeled faintly with FM 1-43. Intermediate cells that responded to positive or bidirectional deflections labeled more consistently with FM 1-43 (Table 1). Finally, we observed that all immature cells with late hair bundles were labeled strongly by FM 1-43 and responded to only positive or bidirectional deflections (Figure 3H; Table 1: 49% bidirectional, 46% positive, 5% no response, n = 39). In morphologically mature hair bundles analyzed at 2 dpf, functional polarity was almost exclusively restricted to the positive direction (Figure 3H; Table 1: 4% bidirectional, 94% positive, 2% no response, n = 51). Collectively, these data indicate that developmental changes in hair-bundle morphology strongly correlate with changes in functional polarity.

Upon establishing a developmental trend in functional polarity, we next sought to confirm that the loss of mechanosensitivity in FM 1-43-unlabeled *ift88*^{tz288b} cells was due to a loss at a specific developmental stage rather than affecting all stages of development. On the whole, we found that compared to wild-type larvae, in *ift88*^{tz288b} mutants the percentage of mechanosensitive cells at 2 dpf was decreased (Table 1: wild-type 89%, n = 188; *ift88* ^{tz288b} 32% n = 72). In wild-type larvae, half of these mechanosensitive cells labeled with FM 1-43 and responded exclusively to positive deflections (Table 1: wild-type 47%, n = 167). In *ift88*^{tz288b} mutants, the vast majority of mechanosensitive cells labeled with FM 1-43 and responded exclusively to positive deflections (Table 1: *ift88* ^{tz288b} 91%, n = 23). These results are consistent with a loss of mechanosensitivity restricted to hair cells that did not label with FM 1-43. Furthermore, in *ift88*^{tz288b} mutants we observed a near absence of mechanosensitive cells at early and intermediate stages of development (Figure 3H; Table 1: wild-type 83%, n = 98; *ift88* ^{tz288b} 11%, n = 36). At these stages, responses to negative deflections were largely abolished in *ift88*^{tz288b} mutants (Figure 3H; Table 1: wild-type 50%; *ift88*^{tz288b} 6%). In addition, at intermediate and late stages, we observed no bidirectional responses (Figure 3H; Table 1: wild-type 34%, n = 90; *ift88*^{tz288b} 0%, n = 33). The occasional responses to negative deflections observed in *ift88*^{tz288b} mutants are likely due to residual *ift88* maternal RNA and the sporadic presence of kinocilia at 2 dpf in these animals (Huang and Schier, 2009). Based on these results, we conclude that kinocilia are not simply acting to couple forces to stereocilia but rather are specifically required for the reversed functional polarity seen in early and intermediate FM 1-43-unlabeled cells and at later stages for the reversed response component of bidirectional responses. Moreover, these data confirm that kinocilia are required for mechanosensitivity during the initial stages of hair-cell development.

Timescale of Functional Polarity Reversal

Although it was clear that kinocilia were required for the reversed functional polarity in immature hair cells, the timescale underlying these functional changes during development was unresolved. To understand the temporal basis of these functional changes, we took advantage of the rapid development of zebrafish hair bundles (bundles develop from early to mature in 14–16 hr) and conducted long-term in vivo imaging by making

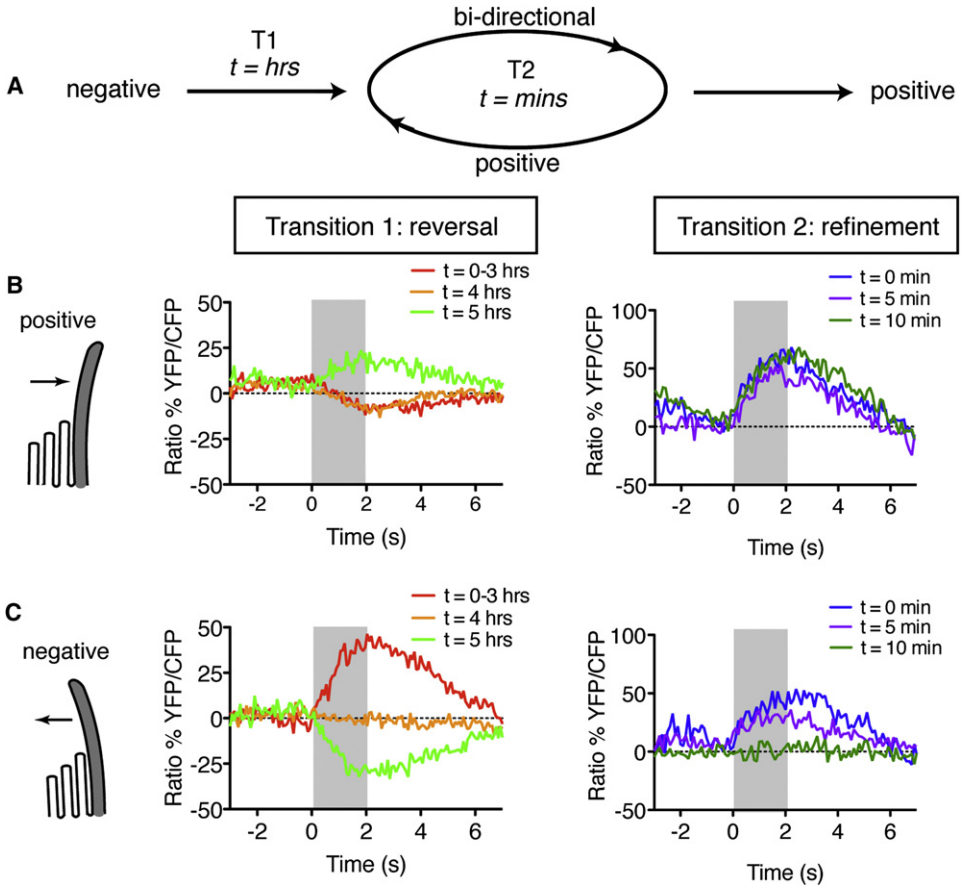

Figure 4. Development of Mature Functional Polarity: First Reversal, Then Refinement

(A) Overall timescale and functional polarity associated with each transition. Early immature cells first go through Transition 1: reversal. During this period, immature cells reverse their functional polarity from the negative to positive direction. Later, immature cells enter Transition 2: refinement. At this stage functional polarity is in rapid flux between bidirectional and positive deflections. Once mature, cells respond to only positive deflections.

(B) Deflection in the positive direction for a cell in Transition 1 (T1) or Transition 2 (T2), respectively.

(C) Deflection in the negative direction for the same cells as in (B).

hourly measurements of functional polarity in developing cells for 5 hr. These experiments identified two transitions in functional polarity during hair cell development (Figure 4A).

The first transition we observed was in immature early cells. Most of these cells remained responsive only to deflections in the negative direction for the entire 5 hr time period (16 of 19). However, 3 of 19 showed a marked functional polarity reversal, transitioning from the negative to the positive direction (Transition 1: Figures 4B and 4C). This transition was relatively slow—it occurred over several hours, and once it occurred, these cells did not revert back to exclusively reversed functional polarity. During this time window we observed no gross changes in cell movements that could account for a reversal in functional polarity. The functional reversal we observed was distinct from previous studies that found sister lateral-line hair cells often rotate after cytokinesis (Wibowo et al., 2011). Postcytokinetic rotation occurs much earlier during development of lateral-line hair cells, prior to when hair cells insert into the apical epithelium and form hair bundles (data not shown).

The second type of transition we observed was in bidirectionally responding cells. Although only 6 of 77 cells responded bidirectionally at the initiation of imaging, 8 additional cells responded bidirectionally at least once over the subsequent 5 hr imaging period. Furthermore, in less than 1 hr, bidirectionally responding cells could change their functional polarity and respond to positive deflections, or vice versa, a phenomenon we observed in 12 of 14 bidirectionally responding cells. By increasing our image acquisition rate, we found that 5 min was sufficient for a cell to convert from bidirectional to positive functional polarity, or vice versa (Transition 2: Figures 4B and 4C), indicating that at this later developmental stage, cells oscillate rapidly between bidirectional and positive unidirectional functional polarity.

Structural Correlates of Kinocilial-Based Mechanosensation

Although we observed a developmental progression in the acquisition of functional polarity, it was unclear how immature, kinocilial-based mechanosensation was functionally distinct

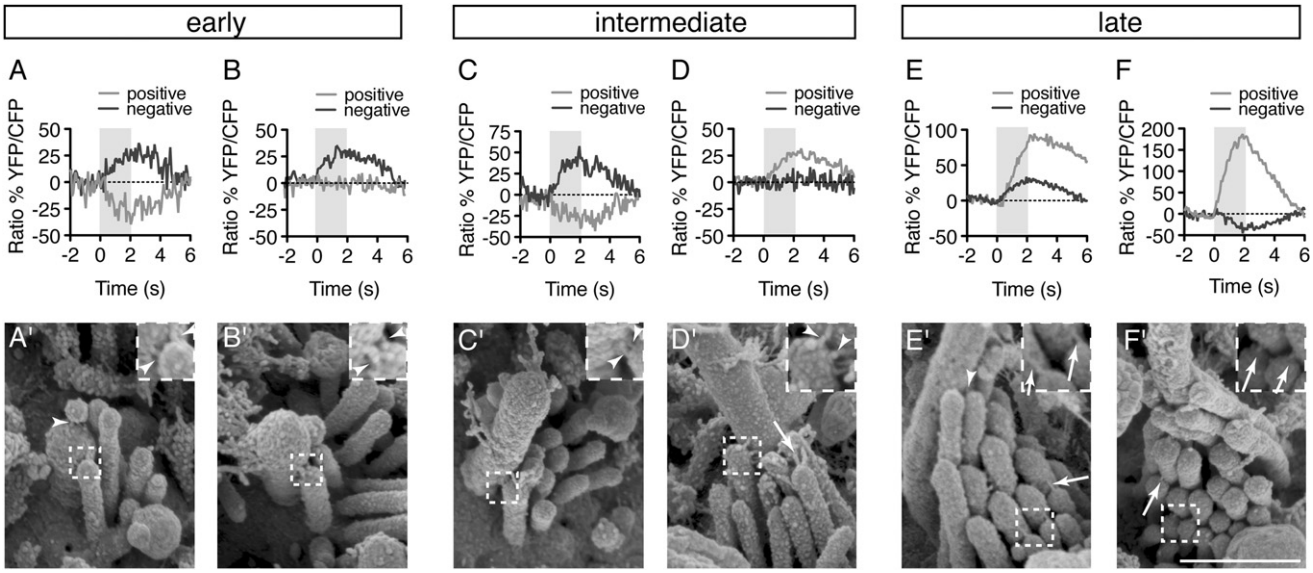

Figure 5. Correlative Calcium Imaging and SEM Reveal a Change in Link Architecture during Development

(A–F) Calcium responses were measured in response to positive and negative hair-bundle deflections from cells at each stage of bundle development.

(A′–F′) SEM images of the hair bundles from hair cells represented in (A)–(F).

All images were taken at 3 dpf. Arrowheads indicate kinocilial links; arrows indicate tip links. Scale bar, 500 nm. Inset is 2× magnification. For additional link examples see also Figure S3.

from traditional stereocilial-based mechanotransduction. To investigate the structural correlates of kinocilial-based mechanosensation, we first recorded mechanically evoked calcium responses in developing hair cells and then used SEM to examine hair-bundle ultrastructure of these same cells (Figure 5).

For these sequential imaging experiments, we examined 6 early, 15 intermediate, and 9 late hair bundles. All cells with early bundles responded to negative deflections and had no detectable tip links (Figures 5A–5B′). SEM imaging demonstrated that half of the early cells had one complete row of stereocilia, and half had bundles with two nearly complete rows (example of a single complete row, Figure 5A′; example of two rows, Figure 5B′; n = 3 with 1 row, n = 3 with 2 rows). In contrast to early cells, cells that responded bidirectionally (Figures 5E and 5E′; n = 3 intermediate, 2 late), or only to positive deflections (Figures 5D, 5D′, 5F, and 5F′; n = 4 intermediate, 7 late), had bundles with detectable tip links. These data demonstrate a correlation between tip-link formation and the acquisition of mature functional polarity.

Our sequential calcium imaging and SEM experiments revealed a structural feature that was common to all stages of development: kinocilial links. On average we observed two kinocilial links radiating from the kinocilia to the tip of each stereocilium (Figures 5A′–5D′ and S4). Linkages were horizontally oriented or slightly oblique with either an upward or downward angle (Figures 5 and S4). This link architecture is quite different than the arrangement observed in the mouse, chick, and bullfrog, where dozens of lateral kinocilial links form a dense network connecting the kinocilium to adjacent stereocilia (Goodyear et al., 2005; Hillman, 1969; Tsuprun et al., 2004).

Because the frequency and location of kinocilial links in zebrafish hair cells appeared more similar to tip links, we reasoned that kinocilial links, via deflection of the kinocilia, might function to gate mechanosensitive channels in immature bundles lacking tip links. Consistent with this hypothesis, *ift88*^{tz288b} hair bundles, which lack mature kinocilia and atypical immature responses, also lack kinocilial links (Figures 2A and 2B). The absence of atypical responses in *ift88*^{tz288b} hair cells and the similarities between zebrafish tip and kinocilial links suggest that kinocilia utilize kinocilial links for their mechanosensitive function.

Kinocilial-Based Mechanosensitivity Is Pharmacologically Similar to Mature, Tip-Link-Based Transduction and Requires Kinocilial Link Components Cdh23 and Pcdh15

To further substantiate a role for kinocilial links in kinocilial-based mechanosensation, we examined zebrafish with null mutations in Cdh23 or Pcdh15, components of tip and kinocilial links. We found that similar to mature hair cells at 5 dpf (Figure S4E), Cdh23 and Pcdh15 were both required for mechanosensitive responses at 2 dpf in hair cells at all stages (Figure 6A: *cdh23* n = 81, *pcdh15* n = 86). In addition, we observed that transient treatment of wild-type hair bundles with 1,2-Bis(2-Aminophenoxy)ethane-*N,N,N′,N′*-tetraacetic acid (BAPTA), which breaks tip and kinocilial links (Assad et al., 1991; Goodyear and Richardson, 2003), also eliminated all responses (Figure 6A). Along with our SEM observations, these results indicate that kinocilial links are part of the gating component required for kinocilial-based mechanosensation in developing hair cells.

Because Cdh23 and Pcdh15 mediate the atypical responses in early cells, we hypothesized that other components of the transduction machinery may be required for reversed functional polarity. To determine if immature, kinocilial-based responses were mediated by a channel similar to that in mature

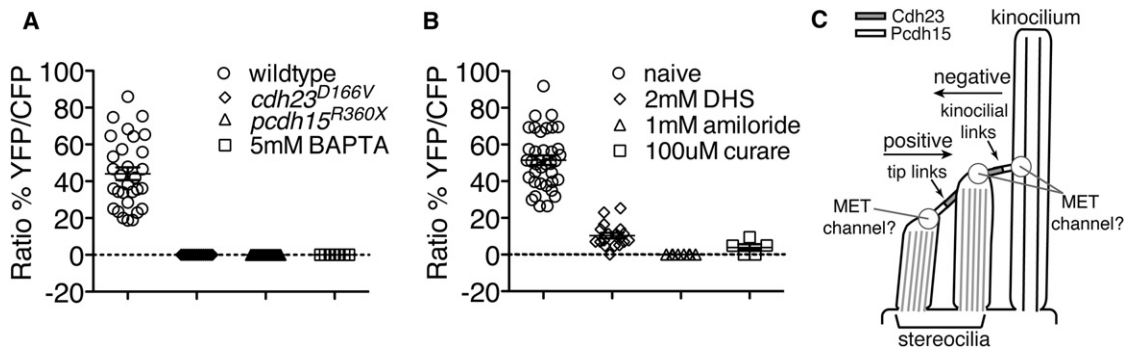

Figure 6. Nascent Hair Cells Require Similar Linkage Components and Channels as Mature Cells

(A) All mutant *cdh23* and *pcdh15* cells at 2 dpf did not respond to stimulation. Treatment of wild-type hair cells with BAPTA also eliminated all responses ($p < 0.001$; $n > 7$ neuromasts).

(B) The mechanotransduction channel blockers amiloride, curare, and DHS significantly blocked responses at 2 dpf ($p < 0.001$; $n > 5$ neuromasts).

(C) Diagram of link asymmetry in hair bundles, and the role of tip links versus kinocilial links in mediating mechanosensitivity in the positive and negative direction, respectively.

Circles indicate potential location for mechanosensitive channels that mediate these responses. An unpaired and paired Student's t tests were used in (A) and (B), respectively. Error bars are SEM.

See also Figure S4.

hair cells, we treated wild-type hair cells with the known mechanotransduction channel blockers dihydrostreptomycin (DHS), amiloride, and curare (Farris et al., 2004). Similar to mature cells at 5 dpf (Figure S4D), each of these channel blockers significantly reduced the response magnitude in all hair cells at 2 dpf (Figure 6B: naive 51.5%, DHS 10.3%, amiloride 0%, curare 3.9%). Although the DHS block was less complete at 2 dpf than at 5 dpf, the degree of inhibition at 2 dpf was independent of FM 1-43 labeling (Figure S4C), suggesting that partial DHS insensitivity may be a general feature of immature hair cells, as previously proposed (Santos et al., 2006). These results suggest that in comparison to tip links, kinocilial-based mechanosensation may utilize a pharmacologically similar mechanosensitive channel.

DISCUSSION

In this study, we investigated whether kinocilia have a mechanosensitive role during hair-cell development by using a combination of noninvasive imaging techniques and ultrastructural analysis. Sequential analysis of function and structure in individual hair cells enabled us to demonstrate the dependence of immature mechanosensitive responses on the kinocilium and its associated linkages.

The use of single-cell in vivo calcium imaging revealed several unexpected findings. First, mechanosensitivity in nascent hair cells initiates much earlier than anticipated—many immature hair cells are mechanosensitive, yet do not label with FM 1-43, a vital dye that permeates mechanotransduction channels. Second, the functional polarity of many FM 1-43-unlabeled hair cells is reversed with respect to the morphological planar polarity of the hair bundle. Third, mechanosensitive responses are detectable before tip links are readily observed and well before hair bundles are fully developed. In these hair cells, the presence of a kinocilium and its associated kinocilial links are required to confer mechanosensitivity. By contrast, mature functional polarity requires tip links. These results suggest that a switch from kinocilial links to tip links underlies changes in functional polarity during development of hair cells.

Molecular Requirements for Reversed Functional Polarity of Immature Hair Cells

In immature hair cells, a kinocilium and kinocilial links tethered to an adjacent stereocilium appear to be sufficient for mediating mechanosensitivity. Because both tip links and kinocilial links are composed of Cdh23 and Pcdh15, the specific requirement for kinocilial links is evident from experiments with *ift88*^{tz288b} mutants. In these mutants, kinocilia are severely stunted and do not form kinocilial links, but bundles of stereocilia with tip links still form and adopt a staircase arrangement similar to wild-type hair bundles (Figure 2B). Yet, in *ift88*^{tz288b} mutant hair cells, there is a striking loss of reversed and bidirectional functional polarity. In contrast, responses to positive deflections are preserved. These results, in tandem with a requirement for Cdh23 and Pcdh15, suggest that early reversed functional polarity, including the reversed component of all bidirectional responses, is mediated by kinocilia and kinocilial links.

Although our experiments show that Pcdh15 and Cdh23 are required for mechanosensitive responses throughout development, it is not apparent how two linkages with the same molecular composition can mediate opposite functional polarities. One major difference between tip links and kinocilial links is in the asymmetric distribution of the cadherins along the plane of functional polarity. For tip links, there is evidence that Pcdh15 is at the lower end, whereas Cdh23 is at the upper end of each linkage (Kazmierczak et al., 2007). This asymmetric distribution is reversed in kinocilial links relative to tip links, with Pcdh15 attached to the kinocilium and Cdh23 attached to adjacent stereocilia (Figure 6C) (Goodyear et al., 2010; Lelli et al., 2010). This reversed asymmetry is intriguing considering the reversed functional polarity of kinocilial-based responses in immature hair cells. In addition to asymmetry of the linkage components

themselves, high-resolution calcium imaging in rat auditory hair cells suggests that mechanotransduction channels are also asymmetrically localized: they are present only at the lower end of each tip link (Beurg et al., 2009). This result is in contrast to an earlier study in bullfrog vestibular hair cells that reported calcium entry into all stereocilia, suggesting that channels may be located at both ends of each link (Denk et al., 1995). Although link asymmetry is an attractive hypothesis to explain immature reversed functional polarity, the location of the mechanotransduction channel may vary according to hair-cell type or species. Whether signaling occurs within the kinocilium or the tallest stereocilium in developing zebrafish hair cells and how this form of mechanosensitivity is functionally reversed await further investigation.

Apart from rat auditory hair cells, the location of the mechanotransduction channel is not known in many vertebrate hair cells. However, pharmacological properties of the channel appear to be conserved across species (Farris et al., 2004; Marcotti et al., 2005; Rüsch et al., 1994; Trapani and Nicolson, 2011). Our data show that similar to mature responses, all immature responses are completely blocked by amiloride and curare but in contrast to mature responses, display partial DHS sensitivity. In addition, the channels of immature cells are FM 1-43 impermeant, suggesting that at least some properties of the mechanotransduction channel differ in kinocilial-based responses. In mature hair cells, sufficient tension in the tip-link-mechanotransduction channel complex maintains a high open probability of the channels (Gale et al., 2001), allowing the permeant channel blockers DHS and FM 1-43 to enter and block channels. Because FM 1-43 does not label immature cells and DHS block is incomplete, it is possible that mechanosensitive channels in these cells may not be open at rest. However, this possibility seems unlikely because sustained deflections in the presence of FM 1-43 failed to produce dye labeling (Figures S4B–S4B‴). In addition, whereas many early immature cells showed an increase in intracellular calcium levels upon negative deflection, they also showed a corresponding decrease in calcium concentration upon positive deflection, consistent with the idea of active channel closure (Figures 5A and 5C). A more likely explanation is that the channels in immature cells are open at rest but possess a unique channel or subunit composition that prohibits FM 1-43 entry and hampers DHS permeability.

Structural and Molecular Changes Underlying the Developmental Progression of Functional Polarity

Short- and long-term imaging of calcium responses in single hair cells revealed that initially, nascent cells are responsive to only negative deflections for several hours before switching to mature or bidirectional functional polarity. The transitional changes in functional polarity are likely to involve both structural and molecular mechanisms. The relatively long interval proceeding the initial switch from reversed functional polarity presumably reflects the time required for large-scale structural maturation of hair bundles, including lengthening of the kinocilium, and the addition of multiple rows of stereocilia and associated tip links (Figures 5A′, 5B′, and 5C′ versus Figures 5D′, 5E′, and 5F′). It is also possible that changes in the angle of kinocilial links during development could account for the responses to negative deflections. For example, in early cells, stereocilia are sometimes taller than the kinocilia, resulting in a downward angle of the link toward the kinocilium (Figure 5A′). This link angle might be optimally oriented for response to negative stimuli. However, we also observed early and intermediate bundles with kinocilia longer than stereocilia; in these cases, the kinocilial links were oriented horizontally or at a slight upward angle, and these cells responded robustly to negative deflections (Figures 5B′ and 5C′). Therefore, there is no apparent correlation between functional polarity and the angle of kinocilial links, and it is unlikely that the angle of this linkage accounts for the developmental changes in functional polarity.

After the initial maturation of the hair bundle and the appearance of tip links, the functional polarity of single cells transitions into a second developmental state in which functional polarity oscillates rapidly within minutes between bidirectional and mature functional polarity. Such fast oscillation is surprising and might be explained by continuous variations in tip-link angle produced during bundle maturation. Variation in the angle of tip links would presumably influence linkage tensioning and ultimately channel activity. However, we did not observe bidirectional responses in *ift88*^{tz288b} mutants in which tip links are unaffected, and therefore this scenario is unlikely. A more consistent explanation is that responses to positive deflections are strictly tip link based, whereas responses to negative deflections within the bidirectional response are kinocilial based. In this situation, rapid fluctuations in functional polarity may be due to a transient loss or gain of kinocilial-based responses. Here, a molecular-based mechanism operating on the same timescale as the fluctuations could account for the rapid changes, such as selective downregulation or posttranslational modification of kinocilial-based mechanotransduction components. Although the exact mechanisms underlying functional polarity reversal are not known at this point, we propose that this process requires a concomitant switch from kinocilial-based to stereocilial-based mechanosensation.

Significance of Kinocilial-Based Mechanotransduction

Similar to other vestibular hair cells, kinocilial links are maintained in mature zebrafish hair cells (Figure S3). However, it is uncertain whether kinocilial-based responses are lost upon maturity or whether they are simply masked by responses generated from tip links. It also seems unlikely that this phenomenon is restricted to zebrafish because both bidirectional and reversed functional polarities have been reported in immature outer hair cells of rat cochlear explants (Waguespack et al., 2007). The presence of kinocilial links in both hair cell types, at least at immature stages, suggests that a developmental progression in the acquisition of functional polarity, mediated in part by the kinocilium, may be a common theme in hair-cell development.

A role for the kinocilium in mechanosensitivity is consistent with many other documented examples of ciliary mechanosensation, such as in kidney epithelial cells and invertebrate mechanoreceptor cells (Kahn-Kirby and Bargmann, 2006; Nauli et al., 2003; Walker et al., 2000). Indeed, it has been hypothesized that the kinocilium is a key structural element underlying the evolution of mechanosensation, as has been studied in single-celled organisms such as the choanoflagellates (Fritzsch et al., 2007).

Although the functional significance of kinocilial-based responses in early developing hair cells is not yet clear, one

early function of kinocilial responses may be in promoting hair cell survival. In zebrafish vestibular hair cells, loss of the kinocilium ultimately results in cell death (Tsujikawa and Malicki, 2004). Interestingly, in mouse auditory cells, specific elimination of kinocilial links also results in degeneration of hair cells (Webb et al., 2011). This degeneration is surprising because mature auditory hair cells do not maintain kinocilia after development. It is therefore possible that calcium signals mediated by kinocilial-based mechanotransduction in immature cells may directly contribute to cell survival or initiate critical differentiation cues, two known important functions of primary cilia signaling in other contexts (Li et al., 2011; Yoshimura et al., 2011).

EXPERIMENTAL PROCEDURES

Zebrafish Husbandry

Zebrafish (*Danio rerio*) were grown at 28°C using standard methods. Animal research was overseen by the Institutional Animal Care and Use Committee at Oregon Health and Sciences University. Larvae were raised in E3 embryo media (5 mM NaCl, 0.17 KCl, 0.33 mM $CaCl_2$ and 0.33 mM $MgSO_4$). Zebrafish mutant alleles used in this study include *cdh23*^{D166V} (*tj264a* allele), *pcdh15*^{R306X} (*th263b* allele), and *ovl*/ *ift88*^{tz288b} and have been described previously (Seiler et al., 2005; Söllner et al., 2004; Tsujikawa and Malicki, 2004). Experiments were performed using the following A-P-oriented lateral-line neuromasts: first otic neuromast, first dorsal, and first four ventral neuromasts of the posterior line.

Vector Construction and Transgenic Lines

Plasmid construction was based on the Tol2/Gateway zebrafish kit (Kwan et al., 2007). The *myo6b* enhancer (Obholzer et al., 2008) was cloned into the 5′ entry vector (p5E, 228); *β-actin* (#BC063950) and cameleon D3cpv (a kind gift from Roger Tsien, University of California, San Diego) (Palmer et al., 2006) were cloned into the middle entry vector (pME, 237). From the tol2 kit, p3E vector containing *GFP* (386) or polyA (302) was recombined with our engineered plasmids to create the following constructs: *myo6b:D3cpv-pA* and *myo6b:β-actin-GFP*. To generate transgenic fish, plasmid DNA and *tol2* transposase mRNA were injected into zebrafish embryos as previously described (Kwan et al., 2007).

Immunofluorescence and Confocal Imaging

A mouse anti-acetylated α-tubulin antibody was used (clone 6-11B-1; Sigma-Aldrich) to stain kinocilia, and Alexa Fluor 568-conjugated phalloidin (Invitrogen) was used to stain hair bundles. Immunohistochemistry was performed on whole-mount larvae following standard immunostaining procedures (see Supplemental Experimental Procedures).

Live and fixed samples were imaged on an upright Zeiss LSM 700 laser-scanning confocal microscope with a 63× 0.95 NA Achroplan or 63× 1.4 NA Plan-Apochromat objective lens, respectively. Excitation wavelengths of 488 nm (GFP or YFP), 555 nm (Alexa 568-conjugated phalloidin or FM 1-43), or 639 nm (Alexa 647-conjugated secondary) were used with a scan rate of 7 μs per pixel with Kalman averaging, 3.0–3.5 optical zoom, and 0.5 μm z sections.

Calcium Imaging

To prepare larvae for calcium imaging, individual larvae were first anesthetized with 0.03% 3-amino benzoic acid ethylester (MESAB, Western Chemical), and pinned onto a SYLGARD-filled recording chamber. To suppress movement, larvae were injected with α-bungarotoxin (125 μM) into the heart. Larvae were then rinsed with extracellular solution (140 mM NaCl, 2 mM KCl, 2 mM $CaCl_2$, 1 mM $MgCl_2$, and 10 mM HEPES [pH 7.3], Osm 310) without MESAB and allowed to recover.

Stimulation of neuromast hair cells has been previously described by Trapani and Nicolson (2011) (also see Supplemental Experimental Procedures). Optical recordings were performed on a Zeiss Axio Examiner upright compound microscope equipped with a Dual-View beam splitter (Optical Insights), a shutter (Sutter Instruments), and an Orca ER CCD camera (Hamamatsu). Fluorescence images were acquired using MetaMorph (Molecular Devices). Acquisitions were taken at 10–20 Hz, with 4 × 4 binning, using a 63× 1.0 NA Plan-Apochromat Zeiss water-immersion objective. Filter/dichroic pairs were as follows: excitation, 420/40; excitation dichroic, 455; CFP emission, 480/30; emission dichroic, 505; YFP emission, 535/30 (Chroma). For information regarding spectral bleed through, photobleaching, and image analysis, see Supplemental Experimental Procedures.

Vital Labeling and Pharmacology

To visualize mature hair cells, larvae were immersed in a 30 μM (2 dpf) or 3 μM (5 dpf) solution of FM 1-43 (Invitrogen) in E3 for 20 s and immediately washed four times in E3. Larvae were imaged by confocal microscopy as described above or by wide-field microscopy with the following filter set: excitation 535/50 565LP and emission 620/60 (Chroma). For quantification of FM 1-43 intensity measurements, the intensity of each neuromast was normalized by the number of FM 1-43-labeled hair cells.

The mechanotransduction blockers DHS, amiloride, and tubo-curarine (curare) (Sigma-Aldrich) were prepared in extracellular solution. For calcium-imaging experiments, the water-jet micropipette solution was also exchanged with extracellular solution containing drug. To cleave tip links, larvae were incubated in 5 mM BAPTA (Invitrogen) in extracellular solution for 10 min and washed thoroughly prior to calcium imaging.

Electron Microscopy

All SEM images were taken of larvae at 3 dpf. This stage is early enough to observe many developing hair bundles but late enough to adequately preserve larvae. For our sequential analysis individual larvae were anesthetized with 0.03% MESAB and pinned onto a SYLGARD-filled chamber. β-*actin-GFP* and FM 1-43 confocal imaging or calcium measurements were performed as described above. After imaging, the cupula surrounding neuromasts was removed by incubating larvae in a high dose of MESAB (0.12%) for 25 s. Specimens were then fixed in 2.5% glutaraldehyde, 2 mM $CaCl_2$ in 0.1 M cacodylate buffer (Electron Microscopy Sciences) for 1.5 hr at room temperature. Samples were washed and postfixed in 80 mM cacodylate buffer containing 50 mM osmium tetroxide (Electron Microscopy Sciences) and 4 mM $CaCl_2$ for 10 min on ice. Embryos were washed twice with water and then dehydrated in steps from 50% to 100% ethanol at room temperature. Larvae were then critical point dried in CO_2 and mounted on carbon-covered aluminum stubs. The head and tail tip of each larvae were painted with silver to minimize charging. Finally, samples were sputter coated with gold palladium. A FEI Sirion XL30 scanning electron microscope was used to acquire images, with a beam strength of 2kV.

Statistical Analysis

A nonparametric Mann-Whitney U test (unpaired) or a Wilcoxon matched-pairs signed rank test (paired) was used to compare differences between populations of hair-cell calcium responses. A t test (paired or unpaired) was used to compare average neuromast calcium responses. A chi-square test was used to compare proportion of hair cells responding or proportion labeling with FM 1-43.

SUPPLEMENTAL INFORMATION

Supplemental Information includes four figures and Supplemental Experimental Procedures and can be found with this article online at http://dx.doi.org/10.1016/j.devcel.2012.05.022.

ACKNOWLEDGMENTS

We thank the Zebrafish International Resource Center for providing *ift88* mutants and Chi-bin Chien at the University of Utah for developing and distributing the zebrafish Tol2 gateway system. We thank Greg Baty at Portland State University's Center for Electron Microscopy and Nanofabrication for assistance with image acquisition, and Kateri Spinelli (OHSU) and Gregory Frolenkov at the University of Kentucky for advice on SEM sample preparation. A. Silk, L. Sheets, and J. Trapani provided useful comments on the manuscript. This research was supported in part by NIH Grant R01

DC006880 and HHMI funding to T.N. and K.S.K. and NIH Training Grant T32 DK 7680-17 to K.S.K.

Received: March 30, 2012
Revised: May 15, 2012
Accepted: May 30, 2012
Published online: August 13, 2012

REFERENCES

Ahmed, Z.M., Goodyear, R., Riazuddin, S., Lagziel, A., Legan, P.K., Behra, M., Burgess, S.M., Lilley, K.S., Wilcox, E.R., Riazuddin, S., et al. (2006). The tip-link antigen, a protein associated with the transduction complex of sensory hair cells, is protocadherin-15. J. Neurosci. *26*, 7022–7034.

Assad, J.A., Shepherd, G.M., and Corey, D.P. (1991). Tip-link integrity and mechanical transduction in vertebrate hair cells. Neuron *7*, 985–994.

Beurg, M., Fettiplace, R., Nam, J.-H., and Ricci, A.J. (2009). Localization of inner hair cell mechanotransducer channels using high-speed calcium imaging. Nat. Neurosci. *12*, 553–558.

Denk, W., Holt, J.R., Shepherd, G.M., and Corey, D.P. (1995). Calcium imaging of single stereocilia in hair cells: localization of transduction channels at both ends of tip links. Neuron *15*, 1311–1321.

Denman-Johnson, K., and Forge, A. (1999). Establishment of hair bundle polarity and orientation in the developing vestibular system of the mouse. J. Neurocytol. *28*, 821–835.

Engström, H., Ades, H.W., and Hawkins, J.E. (1962). Structure and functions of the sensory hairs of the inner ear. J. Acoust. Soc. Am. *34*, 1356–1363.

Farris, H.E., LeBlanc, C.L., Goswami, J., and Ricci, A.J. (2004). Probing the pore of the auditory hair cell mechanotransducer channel in turtle. J. Physiol. *558*, 769–792.

Fritzsch, B., Beisel, K.W., Pauley, S., and Soukup, G. (2007). Molecular evolution of the vertebrate mechanosensory cell and ear. Int. J. Dev. Biol. *51*, 663–678.

Fujiu, K., Nakayama, Y., Iida, H., Sokabe, M., and Yoshimura, K. (2011). Mechanoreception in motile flagella of *Chlamydomonas*. Nat. Cell Biol. *13*, 630–632.

Gale, J.E., Marcotti, W., Kennedy, H.J., Kros, C.J., and Richardson, G.P. (2001). FM 1-43 dye behaves as a permeant blocker of the hair-cell mechanotransducer channel. J. Neurosci. *21*, 7013–7025.

Géléoc, G.S.G., and Holt, J.R. (2003). Developmental acquisition of sensory transduction in hair cells of the mouse inner ear. Nat. Neurosci. *6*, 1019–1020.

Goodyear, R.J., and Richardson, G.P. (2003). A novel antigen sensitive to calcium chelation that is associated with the tip links and kinocilial links of sensory hair bundles. J. Neurosci. *23*, 4878–4887.

Goodyear, R.J., Marcotti, W., Kros, C.J., and Richardson, G.P. (2005). Development and properties of stereociliary link types in hair cells of the mouse cochlea. J. Comp. Neurol. *485*, 75–85.

Goodyear, R.J., Forge, A., Legan, P.K., and Richardson, G.P. (2010). Asymmetric distribution of cadherin 23 and protocadherin 15 in the kinocilial links of avian sensory hair cells. J. Comp. Neurol. *518*, 4288–4297.

Hillman, D.E. (1969). New ultrastructural findings regarding a vestibular ciliary apparatus and its possible functional significance. Brain Res. *13*, 407–412.

Huang, P., and Schier, A.F. (2009). Dampened Hedgehog signaling but normal Wnt signaling in zebrafish without cilia. Development *136*, 3089–3098.

Hudspeth, A.J., and Jacobs, R. (1979). Stereocilia mediate transduction in vertebrate hair cells (auditory system/cilium/vestibular system). Proc. Natl. Acad. Sci. USA *76*, 1506–1509.

Jones, C., Roper, V.C., Foucher, I., Qian, D., Banizs, B., Petit, C., Yoder, B.K., and Chen, P. (2008). Ciliary proteins link basal body polarization to planar cell polarity regulation. Nat. Genet. *40*, 69–77.

Kahn-Kirby, A.H., and Bargmann, C.I. (2006). TRP channels in *C. elegans*. Annu. Rev. Physiol. *68*, 719–736.

Kazmierczak, P., Sakaguchi, H., Tokita, J., Wilson-Kubalek, E.M., Milligan, R.A., Müller, U., and Kachar, B. (2007). Cadherin 23 and protocadherin 15 interact to form tip-link filaments in sensory hair cells. Nature *449*, 87–91.

Kikuchi, K., and Hilding, D.A. (1966). The development of the stria vascularis in the mouse. Acta Otolaryngol. *62*, 277–291.

Kwan, K.M., Fujimoto, E., Grabher, C., Mangum, B.D., Hardy, M.E., Campbell, D.S., Parant, J.M., Yost, H.J., Kanki, J.P., and Chien, C.-B. (2007). The Tol2kit: a multisite gateway-based construction kit for Tol2 transposon transgenesis constructs. Dev. Dyn. *236*, 3088–3099.

Lelli, A., Asai, Y., Forge, A., Holt, J.R., and Géléoc, G.S.G. (2009). Tonotopic gradient in the developmental acquisition of sensory transduction in outer hair cells of the mouse cochlea. J. Neurophysiol. *101*, 2961–2973.

Lelli, A., Kazmierczak, P., Kawashima, Y., Müller, U., and Holt, J.R. (2010). Development and regeneration of sensory transduction in auditory hair cells requires functional interaction between cadherin-23 and protocadherin-15. J. Neurosci. *30*, 11259–11269.

Li, A., Saito, M., Chuang, J.-Z., Tseng, Y.-Y., Dedesma, C., Tomizawa, K., Kaitsuka, T., and Sung, C.H. (2011). Ciliary transition zone activation of phosphorylated Tctex-1 controls ciliary resorption, S-phase entry and fate of neural progenitors. Nat. Cell Biol. *13*, 402–411.

López-Schier, H., Starr, C.J., Kappler, J.A., Kollmar, R., and Hudspeth, A.J. (2004). Directional cell migration establishes the axes of planar polarity in the posterior lateral-line organ of the zebrafish. Dev. Cell *7*, 401–412.

Marcotti, W., van Netten, S.M., and Kros, C.J. (2005). The aminoglycoside antibiotic dihydrostreptomycin rapidly enters mouse outer hair cells through the mechano-electrical transducer channels. J. Physiol. *567*, 505–521.

McGrath, J., Somlo, S., Makova, S., Tian, X., and Brueckner, M. (2003). Two populations of node monocilia initiate left-right asymmetry in the mouse. Cell *114*, 61–73.

Nauli, S.M., Alenghat, F.J., Luo, Y., Williams, E., Vassilev, P., Li, X., Elia, A.E.H., Lu, W., Brown, E.M., Quinn, S.J., et al. (2003). Polycystins 1 and 2 mediate mechanosensation in the primary cilium of kidney cells. Nat. Genet. *33*, 129–137.

Obholzer, N., Wolfson, S., Trapani, J.G., Mo, W., Nechiporuk, A., Busch-Nentwich, E., Seiler, C., Sidi, S., Söllner, C., Duncan, R.N., et al. (2008). Vesicular glutamate transporter 3 is required for synaptic transmission in zebrafish hair cells. J. Neurosci. *28*, 2110–2118.

Palmer, A.E., Giacomello, M., Kortemme, T., Hires, S.A., Lev-Ram, V., Baker, D., and Tsien, R.Y. (2006). Ca2+ indicators based on computationally redesigned calmodulin-peptide pairs. Chem. Biol. *13*, 521–530.

Pickles, J.O., Comis, S.D., and Osborne, M.P. (1984). Cross-links between stereocilia in the guinea pig organ of Corti, and their possible relation to sensory transduction. Hear. Res. *15*, 103–112.

Rüsch, A., Kros, C.J., and Richardson, G.P. (1994). Block by amiloride and its derivatives of mechano-electrical transduction in outer hair cells of mouse cochlear cultures. J. Physiol. *474*, 75–86.

Santos, F., MacDonald, G., Rubel, E.W., and Raible, D.W. (2006). Lateral line hair cell maturation is a determinant of aminoglycoside susceptibility in zebrafish (*Danio rerio*). Hear. Res. *213*, 25–33.

Schwander, M., Kachar, B., and Müller, U. (2010). Review series: the cell biology of hearing. J. Cell Biol. *190*, 9–20.

Seiler, C., Finger-Baier, K.C., Rinner, O., Makhankov, Y.V., Schwarz, H., Neuhauss, S.C.F., and Nicolson, T. (2005). Duplicated genes with split functions: independent roles of protocadherin15 orthologues in zebrafish hearing and vision. Development *132*, 615–623.

Shin, J.B., Adams, D., Paukert, M., Siba, M., Sidi, S., Levin, M., Gillespie, P.G., and Gründer, S. (2005). *Xenopus* TRPN1 (NOMPC) localizes to microtubule-based cilia in epithelial cells, including inner-ear hair cells. Proc. Natl. Acad. Sci. USA *102*, 12572–12577.

Shotwell, S.L., Jacobs, R., and Hudspeth, A.J. (1981). Directional sensitivity of individual vertebrate hair cells to controlled deflection of their hair bundles. Ann. N Y Acad. Sci. *374*, 1–10.

Si, F., Brodie, H., Gillespie, P.G., Vazquez, A.E., and Yamoah, E.N. (2003). Developmental assembly of transduction apparatus in chick basilar papilla. J. Neurosci. *23*, 10815–10826.

Siemens, J., Lillo, C., Dumont, R.A., Reynolds, A., Williams, D.S., Gillespie, P.G., and Müller, U. (2004). Cadherin 23 is a component of the tip link in hair-cell stereocilia. Nature *428*, 950–955.

Söllner, C., Rauch, G.J., Siemens, J., Geisler, R., Schuster, S.C., Müller, U., and Nicolson, T.; Tübingen 2000 Screen Consortium. (2004). Mutations in cadherin 23 affect tip links in zebrafish sensory hair cells. Nature *428*, 955–959.

Tanaka, K., and Smith, C.A. (1978). Structure of the chicken's inner ear: SEM and TEM study. Am. J. Anat. *153*, 251–271.

Tanimoto, M., Ota, Y., Inoue, M., and Oda, Y. (2011). Origin of inner ear hair cells: morphological and functional differentiation from ciliary cells into hair cells in zebrafish inner ear. J. Neurosci. *31*, 3784–3794.

Tilney, L.G., Tilney, M.S., and DeRosier, D.J. (1992). Actin filaments, stereocilia, and hair cells: how cells count and measure. Annu. Rev. Cell Biol. *8*, 257–274.

Trapani, J.G., and Nicolson, T. (2011). Mechanism of spontaneous activity in afferent neurons of the zebrafish lateral-line organ. J. Neurosci. *31*, 1614–1623.

Tsujikawa, M., and Malicki, J. (2004). Intraflagellar transport genes are essential for differentiation and survival of vertebrate sensory neurons. Neuron *42*, 703–716.

Tsuprun, V., Goodyear, R.J., and Richardson, G.P. (2004). The structure of tip links and kinocilial links in avian sensory hair bundles. Biophys. J. *87*, 4106–4112.

Waguespack, J., Salles, F.T., Kachar, B., and Ricci, A.J. (2007). Stepwise morphological and functional maturation of mechanotransduction in rat outer hair cells. J. Neurosci. *27*, 13890–13902.

Walker, R.G., Willingham, A.T., and Zuker, C.S. (2000). A Drosophila mechanosensory transduction channel. Science *287*, 2229–2234.

Webb, S.W., Grillet, N., Andrade, L.R., Xiong, W., Swarthout, L., Della Santina, C.C., Kachar, B., and Müller, U. (2011). Regulation of PCDH15 function in mechanosensory hair cells by alternative splicing of the cytoplasmic domain. Development *138*, 1607–1617.

Wibowo, I., Pinto-Teixeira, F., Satou, C., Higashijima, S., and López-Schier, H. (2011). Compartmentalized Notch signaling sustains epithelial mirror symmetry. Development *138*, 1143–1152.

Yoshimura, K., Kawate, T., and Takeda, S. (2011). Signaling through the primary cilium affects glial cell survival under a stressed environment. Glia *59*, 333–344.